X-ray Talbot-Lau Interferometer for High-Speed Phase Imaging at BL-14C

Margie P. OLBINADO[1*], Sebastien HARASSE[1**], Wataru YASHIRO[1*] and Atsushi MOMOSE[1*]

[1]Department of Advanced Materials Science, Graduate School of Frontier Sciences, the University of Tokyo
[*]Current affiliation:Institute of Multidisciplinary Research for Advanced Materials, Tohoku University,
[**]Current affiliation: The CS group

Abstract

A Talbot-Lau interferometer for high-speed x-ray phase imaging using white synchrotron radiation was constructed at BL-14C, allowing for the vertical sample rotation axis during tomography. The distances of the gratings were set optimum for 28.8 keV x-rays. An average moiré fringe visibility of 20% was observed. High speed tomography of a polymer sphere was demonstrated via the Fourier transform method at 500 projections/ sec. The results show the feasibility of four-dimensional imaging of non-rigid and fluid samples at a time resolution of 1 second.

1. Introduction

X-ray phase imaging is a valuable tool in examining soft materials which exhibit poor contrast in conventional x-ray absorption imaging. This is because for low-Z elements, the x-ray scattering cross section which is responsible for x-ray phase shifts is a thousand times larger than the absorption cross section. A review on the advances in x-ray phase imaging has been presented in Ref. 1. Over the years, various techniques to detect and measure the x-ray phase shift have been developed especially in synchrotron facilities where highly brilliant x-rays are available [1]. In particular, the techniques which utilize crystal optics such as crystal interferometers and refraction-based methods require collimated monochromatic x-rays hence brilliant synchrotron x-rays are necessary in order to acquire images at a practical exposure time.

In contrast with the crystal-based techniques, polychromatic x-rays can be used for grating-based and propagation-based methods [2, 3, 4]. This proves to be very advantageous in advancing the x-ray imaging field towards fast imaging of dynamic phenomena which has been performed by taking advantage of the high flux of white beam synchrotron radiation. X-ray phase contrast imaging by edge-enhancement through propagation-based method to study the flow dynamics of dense liquid jets has been reported [5]. Using the x-ray Talbot interferometer with white beam synchrotron not only high-speed x-ray phase contrast imaging has been accomplished, but time-resolved x-ray phase tomography has also been performed [6, 7].

Fig. 1(a) shows the set-up of the x-ray Talbot interferometer for high-speed x-ray differential phase imaging and x-ray phase tomography utilizing white synchrotron radiation at BL-14C. It is typically composed of a π/2 phase grating (G_1) with pitch d_1 and an amplitude grating (G_2) with pitch d_2. Assuming plane-wave illumination of spatially coherent x-rays along the z-axis

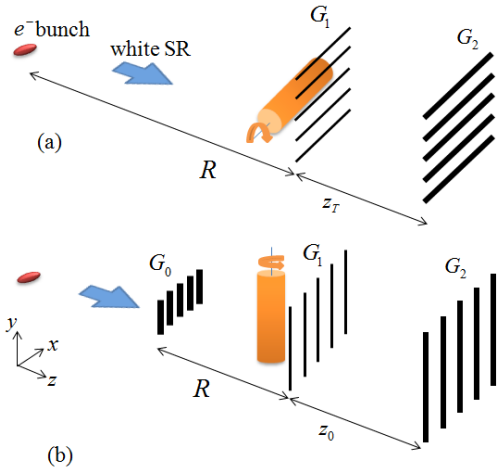

Figure 1 (a) X-ray Talbot interferometer and (b) X-ray Talbot-Lau interferometer set-up at the BL-14C.

and gratings parallel to the x-y plane with its grating lines along the x-axis, G_1 produces self-images for each wavelength of x-ray λ at distances $z_T(\lambda) = pd_1^2/\lambda$ from G_1, where p is the fractional Talbot order which is an odd multiple of 1/2 for a π/2 phase grating [8]. A phase object placed just in front of G_1 slightly refracts the beam and distorts the self-image. When G_2 is placed at z_T, a moiré pattern is generated and the intensity distribution is:

$$I(x,y;\lambda) = \sum_n a_n(\lambda)\exp\left[2\pi n i \frac{z_T(\lambda)}{d_1}\varphi_y(x,y;\lambda)\right] \qquad (1)$$

where the coefficients $a_n(\lambda)$ are dependent on the gratings' transmission function and the spatial coherence of the x-rays. The moiré pattern is a superposition of the self-image of G_1 with the pattern of G_2. The beam deflection $\varphi_y(x, y; \lambda)$ in the y-direction at G_2 is related to the gradient of the phase shift $\Phi(x, y; \lambda)$ of the x-rays passing through the phase object with

refractive index 1 - δ (x, y, z; λ) placed just in front of G_1:

$$\varphi_y(x,y;\lambda) = \frac{\lambda}{2\pi}\frac{\partial\Phi(x,y;\lambda)}{\partial y} \quad , \qquad (2)$$

where

$$\Phi(x,y;\lambda) = \frac{2\pi}{\lambda}\int \delta(x,y,z;\lambda)dz. \qquad (3)$$

Taking into account the spectrum of the x-rays, the resultant moiré pattern is:

$$\widetilde{I}(x,y) = \int d\lambda P(\lambda) I(x,y;\lambda) \qquad (4)$$

where $P(\lambda)$ is the normalized spectrum function of x-rays. In this case, the measured differential phase is considered to be an average differential phase image. From the resulting distorted moiré patterns, the differential phase shift due to the sample can be obtained using the phase-stepping technique [2] or the Fourier transform method [6].

Theoretically, for a π/2 phase grating as G_1, the image would be comparable to that obtained using monochromatic x-rays for a spectral bandwidth $\Delta\lambda/\lambda < 1/8$ [2]. In the previous high-speed x-ray phase imaging that has been performed using a Talbot interferometer with white synchrotron radiation the spectral bandwidth was larger than 1/8 but phase imaging and tomography was demonstrated although with reduced image quality [6, 7].

To generate the Talbot effect the spatial coherence length of x-rays must be larger than pd_1 [2]. The spatial coherence length of x-rays at a distance R from a source having a Gaussian intensity distribution is given by $L_{coh} = \lambda R/2\pi\sigma$, where σ is the standard deviation of the Gaussian distribution and λ is the wavelength of the x-rays. At the Photon Factory, the horizontal and vertical standard deviation of the electron bunches in the storage ring are 45 μm and 570 μm, respectively. These correspond to $L_{coh,\ y}$ = 5.6 μm and $L_{coh,\ x}$ = 0.44 μm at the location of the Talbot interferometer which is 37 m from the source. Hence, the gratings of the Talbot interferometer for p = 1/2 had to be oriented horizontally as illustrated in Fig. 1(a).

In many cases a vertical sample rotation axis is preferable for tomography to eliminate the motion blur due to gravity during rotation. Moreover, for observations of dynamic phenomena in fluids the sample rotation axis has to be vertical. To utilize our Talbot interferometer in these cases, the sample rotation axis would have to be perpendicular to the gratings. In x-ray phase tomography, the differential phase is integrated to obtain the phase shift Φ (x, y) followed by the conventional filtered back-projection technique to obtain δ (x, y, z) [2], or alternatively, by reconstructing δ (x, y, z) from plural projections of the differential phase using the modified filtered back-projection [9, 10]. The phase shift outside the sample region is assumed to be zero. If there is no such region along the line of integration, the calculation of the phase shift and the reconstruction of the tomograms become cumbersome. For these kinds of samples, it is necessary to use a configuration in which both the sample rotation axis and grating lines are vertical. Hence, in this work an X-ray Talbot-Lau interferometer [11, 12] was constructed to increase the spatial coherence of the x-rays along the horizontal allowing for the vertical orientation of the gratings and the sample rotation axis during tomography.

2. X-ray Talbot-Lau Interferometer Set-up

Fig. 1(b) illustrates the x-ray Talbot-Lau interferometer set-up. It is composed of three gratings: a source grating (G_0), a phase grating (G_1) and an amplitude grating (G_2). The opening width of G_0 must be small enough to produce vertically spatially coherent x-rays for G1 to exhibit the Talbot effect. The distance between G_0 and G_1 is $R = pd_0d_1/\lambda$ and the pitch of source grating d_0 must satisfy the ratio $d_0 : R = d_2 : z_0$ and so that the self-images of G_1 superimpose constructively. In this configuration, the distance between G_1 and G_2 is $z_0 = pd_1d_2/\lambda$ and the pitch d_2 must satisfy the ratio $d_2 : d_1 = (R+z_0) : R$ [13, 14].

The Talbot-Lau interferometer was constructed at BL-14C. We utilized a white synchrotron radiation from a 5-Tesla vertical wiggler installed in the 2.5-GeV storage ring operating at 50 mA ring current (single-bunch mode). The periods of G_0, G_1 and G_2 were 30 μm, 4.5 μm and 5.3 μm, respectively. The opening line width of G_0 was 10 μm and the thickness of the gold lines was 100 μm. The area of the source grating was 5 mm × 5 mm. The distances between the gratings were chosen so that 28.8 keV x-rays are optimal: z_0 = 277 mm and R = 1.57 m given the fractional Talbot order p = 1/2.

The visibility $V = (I_{max} - I_{min}) / (I_{max} + I_{min})$ of the moiré fringes for each detector pixel and the standard deviation of the moiré phase shift were calculated via the fringe scanning technique. A five-step fringe scan was performed by moving G_2 across one period of the G_1 self-image. The exposure time for each moiré image was 1.96 msec. The smallest detectable beam deflection was calculated from the standard deviation of the moiré phase shift.

To demonstrate the Talbot-Lau interferometer for high-speed tomography, we employed the Fourier transform method to obtain the differential phase images of a polyethylene (PE) sphere of 3.2-mm diameter. G_2 was tilted against G_1 to generate the carrier fringes. 500 projections were obtained as the sample was rotated by 360º in 1 second. The exposure time for each projection was 1.96 msec. We used an x-ray image detector composed of a 20 μm-thick $Y_3Al_5O_{12}$:Ce phosphor screen (P46 Hamamatsu), a coupling lens system (AA60, Hamamatsu) and a CMOS camera (pco.dimax, PCO AG). The measured effective pixel size of the detector system was 11.2 μm.

3. Results and Discussion

An image of the moiré fringes generated by the x-ray Talbot-Lau interferometer is shown in Fig. 2(a). The average visibility of the fringes was 20%. The calculated moiré phase shift due to the PE sphere is shown in Fig. 2(b), which was obtained by the fringe-scanning technique. The standard deviation of the moiré phase is 0.07 rad corresponding to 0.2 μrad smallest beam deflection that can be detected by the Talbot-Lau interferometer. The grayscale corresponds to ±3.0 μrad beam deflection. The spatial resolution based on the FWHM of the differential contrast profile at the sample edge is 22 μm.

Fig. 3(a) shows the generated moiré fringes to detect the differential phase shift introduced by polyethylene sample. The carrier fringe period was 75 μm and the visibility of the carrier fringes was 8.3%. It was slightly inclined from the horizontal because only G_2 was tilted ($\theta \approx 0.10$ rad) to generate the fringe. The carrier fringe frequency f_y used in the Fourier transform was then equal to $f/\cos(\theta/2)$ but this modification was negligible. The differential phase image obtained using the Fourier transform method is shown in Fig. 3(b). The standard deviation of the moiré phase is 0.1 rad corresponding to 0.8 μrad beam deflection that can be detected by the Talbot-Lau interferometer. The grayscale corresponds to ±3.0 μrad of beam deflection.

Fig. 4 shows a slice of the reconstructed refractive index decrement $\delta(x, y, z)$ of the polyethylene sample indicated by the dashed line in Fig. 3(b). The experimentally obtained average refractive index difference for the polyethylene sample in air is 2.5 (± 0.2) × 10^{-7}. The theoretical value of δ of polyethylene is 2.53 × 10^{-7} assuming 28.8 keV x-rays. The grayscale corresponds to a refractive index difference range of 0 to 3.0 × 10^{-7}. The circular artifact in the tomogram indicated by the arrow is a remnant of the high frequency filtering that was performed on the sinograms. Fig. 5 (a) shows the corresponding sinogram of the slice in Fig. 4. The vertical axis of the sinogram denotes a time interval of 0.5 sec corresponding to 250 projections for a 180° sample turn. High-spatial frequency filtering was employed to remove the vertical lines which were caused by the defects on the gratings. However, the sinogram also has high spatial frequency components at the edges of the sample. As a result vertical lines tangent to the edges are present after filtering which can be observed on the corrected sinogram in Fig. 5(b). To avoid this problem, it is important to have high quality gratings.

The horizontal bright and dark bands can also be observed in the sinogram. This indicates a changing background

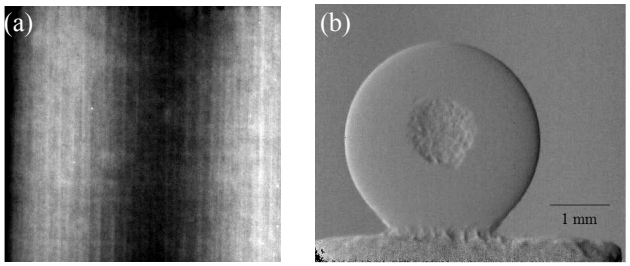

Figure 2 (a) Moiré fringe and (b) moiré phase shift image of the PE sphere.

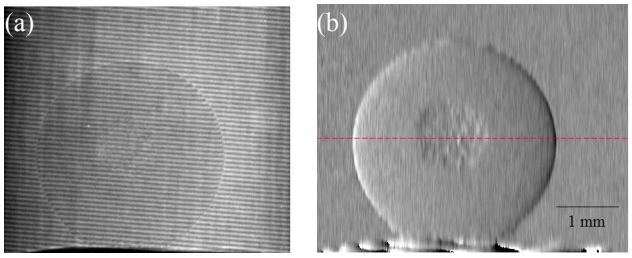

Figure 3 (a) Fine moiré fringes generated to obtain the (b) differential phase image of the PE sphere via Fourier transform method.

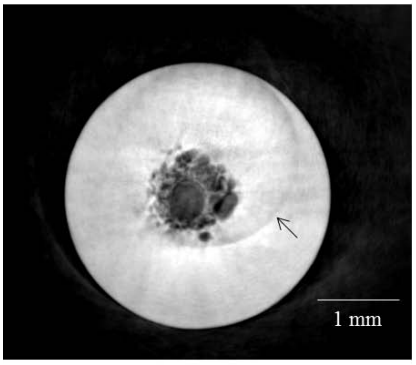

Figure 4 Tomogram slice of the reconstructed $\delta(x, y, z)$ of the PE sphere.

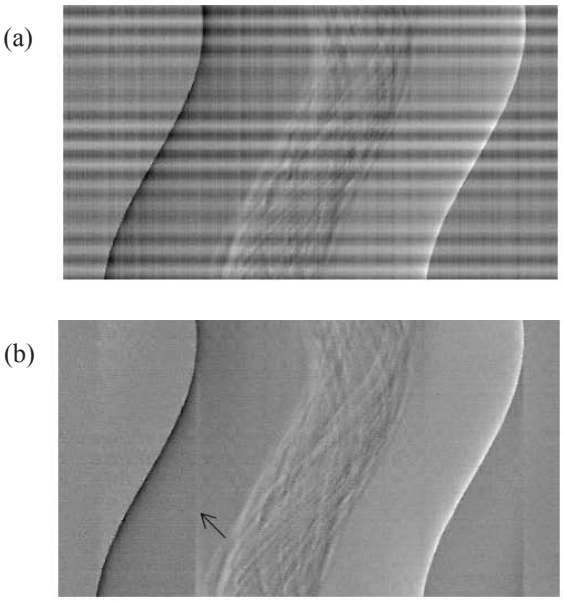

Figure 5 Corresponding (a) sinogram and (b) denoised sinogram of the tomogram slice of the PE sphere in Fig. 4.

moiré phase caused by vibrating moiré fringe which was inferred to be due to the vibration of the gratings. It is easy to correct this noise because the vibration of the moiré was recorded in each differential phase image since the camera frame rate was faster than the vibration. The oscillating background differential phase was subtracted from the sinogram by assuming that the background differential phase shift was zero. The frequencies of vibration were 16 Hz and 28 Hz hence an observed beat pattern of vibration. The relative displacement of the gratings during vibration was quantified to be a few microns. To improve the imaging system, it is important to address this mechanical stability.

4. Conclusion

We have constructed an x-ray Talbot-Lau interferometer for high-speed x-ray phase imaging and tomography using white synchrotron radiation in BL-14C. The vertical source grating that was utilized has successfully increased the horizontal spatial coherence of the synchrotron radiation for the operation of the Talbot-Lau interferometer with its gratings in vertical orientation allowing for the sample rotation axis to be vertical. This vertical orientation is desirable for dynamic X-ray phase imaging of non-rigid samples and fluids. The gratings were set for an optimum x-ray energy of 28.8 keV. The average visibility of the fringes was 20%. The interferometer was successfully demonstrated for high-speed x-ray phase tomography of a polyethylene sphere at 0.5 sec/tomogram. The mechanical stability of the system should be addressed and better quality gratings could be used to improve the quality of the images. We have plans to perform four-dimensional X-ray phase tomography with a time resolution of 1 second using this system.

Acknowledgements

We thank Prof. T. Hattori for the grating fabrication. We also appreciate the technical support by Dr. K. Hyodo. This experiment was performed under the approval number 2011G037. This research was supported by JST-SENTAN.

References

[1] A. Momose, *Jpn. J. Appl. Phys*. **44** 6355- 6367 (2005).

[2] A. Momose, W. Yashiro, Y. Takeda, Y. Suzuki, and T. Hattori, *Jpn. J. Appl. Phys*. **45**, 5254-5262 (2006).

[3] T. Weitkamp, A. Diaz, C. David, F. Pfeiffer, M. Stampanoni, P. Cloetens, and E. Ziegler, *Opt. Express* **13**, 6296-6304 (2005).

[4] S. W. Wilkins, T. E.Gureyev, D. Gao, A. Pogany, and A. W. Stevenson, *Nature* **384**, 335–338 (1996).

[5] Y. Wang, X. Liu, K. S. Im, W. K. Lee, J. Wang, K. Fezzaa, *Nat. Phys*. **4**, 305-309 (2008).

[6] A. Momose, W. Yashiro, H. Maikusa, and Y. Takeda, *Opt. Express* **17**, 12540-12545 (2009).

[7] A. Momose, W. Yashiro, S. Harasse, and H. Kuwabara, *Opt. Express* **19**, 8423-8432 (2011).

[8] P. Cloetens, J. P. Guigay, C. De Martino, J. Baruchel, and M. Schlenker, *Opt. Lett*. **22**, 1059-1061 (1997).

[9] G. W. Faris and R. L. Byer, *Appl. Opt*. **27**, 5202-5212 (1988).

[10] F. Pfeiffer, C. Kottler, O. Bunk, and C. David, *Phys. Rev. Lett.* **98**, 108105 (2007).

[11] J. F. Clauser and M. W. Reinsch, *Appl. Phys*. B **54** 380-395 (1992).

[12] F. Pfeiffer, T. Weitkamp, O. Bunk, and C. David, *Nat. Phys*. **2**, 258-261 (2006).

[13] K. Patorski, *Progress in Optics* XXVII (Elsevier, Amsterdam, 1989) Chap. I.

[14] W. Yashiro, Y. Takeda, and A. Momose, J. *Opt. Soc.Am. A* **25**, 2025-2039 (2008).

（原稿受付日：2012 年 6 月 29 日）

Margie P. OLBINADO
Institute of Multidisciplinary Research for Advanced Materials, Tohoku University
2-1-1, Katahira, Aoba-ku, Sendai 980-8577, Japan
Tel & Fax: 022-217-5107
E-mail: olbinado@mml.k.u-tokyo.ac.jp, olbinado@mail.tagen.tohoku.ac.jp

Sebastien HARASSE
the CS Group
5 rue Brindejonc des Moulinais, 31506 Toulouse Cedex 5, France.
Tel : +33561176331
E-mail : sebastien.harasse@c-s.fr

Wataru YASHIRO
Institute of Multidisciplinary Research for Advanced Materials, Tohoku University
2-1-1 Katahira, Aoba-ku, Sendai 980-8577, Japan
Tel & Fax: 022-217-5107
E-mail: wyashiro@tagen.tohoku.ac.jp

Atsushi MOMOSE
Institute of Multidisciplinary Research for Advanced Materials, Tohoku University
2-1-1 Katahira, Aoba-ku, Sendai 980-8577, Japan
Tel: 022-217-5388　Fax: 022-217-5826
E-mail: momose@tagen.tohoku.ac.jp